JACS
JOURNAL OF THE AMERICAN CHEMICAL SOCIETY
Article
Cite This: J. Am. Chem. Soc. 2019, 141, 4080−4085
pubs.acs.org/JACS

Spatially Selective and Density-Controlled Activation of Interfacial Mechanophores

Audrey R. Sulkanen,[†,#] Jaeuk Sung,[‡,∥,#] Maxwell J. Robb,[§,∥,⊥] Jeffrey S. Moore,[‡,§,∥] Nancy R. Sottos,*[,‡,∥] and Gang-yu Liu*[,†]

[†]Department of Chemistry, University of California, Davis, California 95616, United States
[‡]Materials Science and Engineering, [§]Department of Chemistry, and [∥]Beckman Institute for Advanced Science and Technology, University of Illinois Urbana−Champaign, Urbana, Illinois 61801, United States
[⊥]Division of Chemistry and Chemical Engineering, California Institute of Technology, Pasadena, California 91125, United States

Supporting Information

ABSTRACT: Mechanically sensitive molecules known as mechanophores have recently attracted much interest due to the need for mechanoresponsive materials. Maleimide−anthracene mechanophores located at the interface between poly(glycidyl methacrylate) (PGMA) polymer brushes and Si wafer surfaces were activated locally using atomic force microscopy (AFM) probes to deliver mechanical stimulation. Each individual maleimide−anthracene mechanophore exhibits binary behavior: undergoing a retro-[4 + 2] cycloaddition reaction under high load to form a surface-bound anthracene moiety and free PGMA or remaining unchanged if the load falls below the activation threshold. In the context of nanolithography, this behavior allows the high spatial selectivity required for the design and production of complex and hierarchical patterns with nanometer precision. The high spatial precision and control reported in this work brings us closer to molecular level programming of surface chemistry, with promising applications such as 3D nanoprinting, production of coatings, and composite materials that require nanopatterning or texture control as well as nanodevices and sensors for measuring mechanical stress and damage in situ.

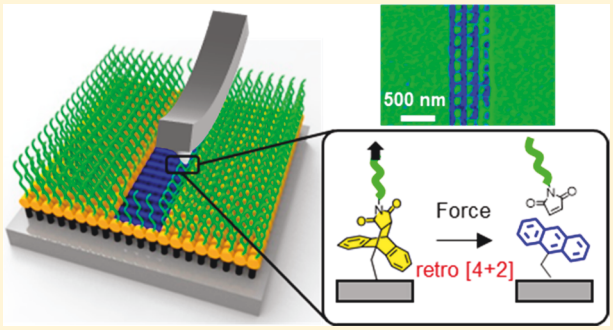

INTRODUCTION

Polymer mechanochemistry has attracted much interest recently in order to understand the fundamental scientific questions of force activation of chemical change as well as for its technological potential related to the preparation of mechanoresponsive materials.[1−4] Mechanically sensitive molecules known as mechanophores are activated via force to trigger desirable chemical transformations such as color changes,[5−7] catalytic reactions,[8] depolymerization,[9] small molecule release,[10] and changes in electrical conductivity.[11] Immobilizing mechanophores on solid surfaces has provided new opportunities for producing functional materials with responsive interfaces such as polymer−silica particles,[12] polymer−cellulose,[13] and silk−epoxy materials[14] and for applications including fabrication of sensors and nanodevices.

Commonly reported means of activation include applying mechanical forces to bulk polymeric materials,[6,15,16] ultrasonicating dilute polymer solutions,[17−19] or performing single-molecule force spectroscopy on surface-bound polymers.[20−24] More recently, a laser-spallation technique was utilized to activate and characterize mechanochemical transformations at a solid interface.[25] While previous approaches are effective at triggering activation, methods that enable nanometer spatial precision are critical for producing custom-designed structures as well as fabricating nanocomposite materials and nanodevices with desired structural, physical, and chemical properties.

Atomic force microscopy (AFM) is known for its molecular resolution in imaging and lithography.[26,27] In addition, AFM operates in various environments, including ultrahigh-vacuum, ambient, and solution environments, and, as such, is versatile enough to accommodate a wide range of chemical reactions.[28−30] Furthermore, AFM enables accurate force control over a wide range: from pN to hundreds of μN in one experimental setup.[30−33] The local pressure at contact is tunable from kPa to GPa.[34] Finally, AFM enables surface nanolithography as well as structural characterization in situ.[35−38] Previously, AFM has been used as a nanolithography tool to pattern self-assembled monolayers (SAMs) such as alkanethiols on precious metals,[37,39,40] silanes on Si wafers and glass,[41] and polymers.[27,42]

This work reports using AFM probes to activate mechanochemical reactions at interfaces. Taking advantage of the spatial precision and force tunability of AFM, this approach

Received: December 19, 2018
Published: February 12, 2019

DOI: 10.1021/jacs.8b10257
J. Am. Chem. Soc. 2019, 141, 4080−4085

affords excellent control over the spatial activation of mechanochemical reactions on surfaces. This level of control over interfacial reactions enables the fabrication of complex structures with nanometer precision and signifies a critical step toward programming surface chemistry molecule-by-molecule. The outcomes of our experiments demonstrate the feasibility for controlling mechanophore-based surface chemical reactions, 3D nanoprinting, and production of advanced coatings and composite materials that require nanopatterning or texture control as well as nanodevices and sensors for mechanical stress and damage in situ.[1,2,43−45]

RESULTS AND DISCUSSION

Spatially Selective Activation of Interfacial Mechanophores. The concept of spatially selective activation is illustrated in Figure 1, using the well-known maleimide−anthracene (MA) mechanophore. The MA mechanophore has been reported by us[12,46] and others[47,48] to undergo a mechanically activated retro-Diels−Alder reaction (retro-[4 + 2] cycloaddition) to form maleimide and anthracene in solution and at nanoparticle−liquid interfaces. In this work, MA mechanophores were immobilized on a Si wafer surface via alkyl−siloxane self-assembly,[49] and a poly(glycidyl methacrylate) (PGMA) brush was grown subsequently. The interfacial MA mechanophore activation was monitored in situ by measuring the decrease in topographic height after high contact force application. Synthesis of surface-bound MA mechanophores has been reported in previous literature, and the formation of polymer brushes on Si wafers is described in detail in the Supporting Information (SI).

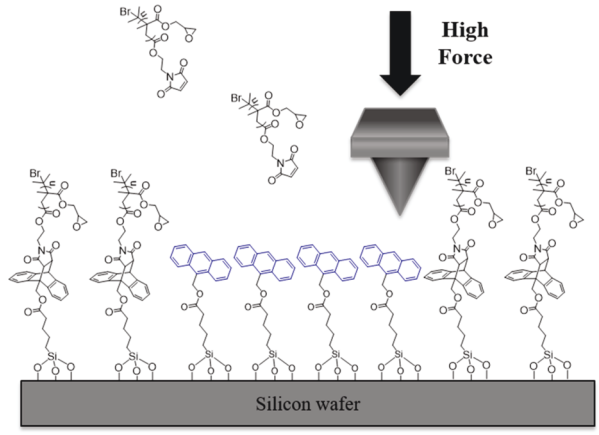

Figure 1. Activation of MA mechanophores at the interface between a polymer brush and silicon surface using an AFM probe. Each mechanophore activation produces a free maleimide and a surface-bound anthracene group via a retro-[4 + 2] cycloaddition reaction.

The imaging and activation of the MA mechanophore was achieved in three steps. The mechanophore-functionalized polymer brush surface was first imaged in dimethyl sulfoxide (DMSO) in contact mode via AFM under a gentle force, e.g., 10 nN, or 0.35 GPa, pressure estimated using Hertzian contact mechanics.[30,34] Upon selecting the activation region, the AFM probe was moved to the designated location, and the contact force was increased, e.g., to 350 nN, or 1.16 GPa. During the scan, molecules underneath the probe were subject to vertical pressure as well as lateral shear. The combined local mechanical perturbation is known to break van der Waals interactions, hydrogen bonds, chemisorbed species,[37,50,51] and ionic and covalent bonds.[52] Given that each MA mechanophore is specifically designed to undergo a force-activated retro-Diels−Alder reaction,[12] we envision a force range that could selectively activate the mechanophore without inducing scission of the covalent bonds in each polymer brush. The proof of this concept paves the way to generate locally defined patterns that are chemically differentiated according to the scanning trajectory of the AFM probe.

Our experimental studies had to first address variations in probe apexes by determining an activation threshold for each experiment. The threshold value was found by scanning a test area with systematically increasing loads. After high-load scanning of a designated area, the load was reduced to a low force, e.g., 10 nN, and the region was reimaged for changes in the surface morphology (Figure 1). The outcome and spatial selectivity of each high-load scan was successfully characterized by AFM, in situ, as each activation event cleaves a polymer strand, reducing the layer's height by a measurable degree and exposing surface-bound anthracene. To confirm that the mode of activation was via the retro-Diels−Alder reaction, the substrates were examined by fluorescence microscopy, as anthracene exhibits characteristic emission at 420 nm.[47]

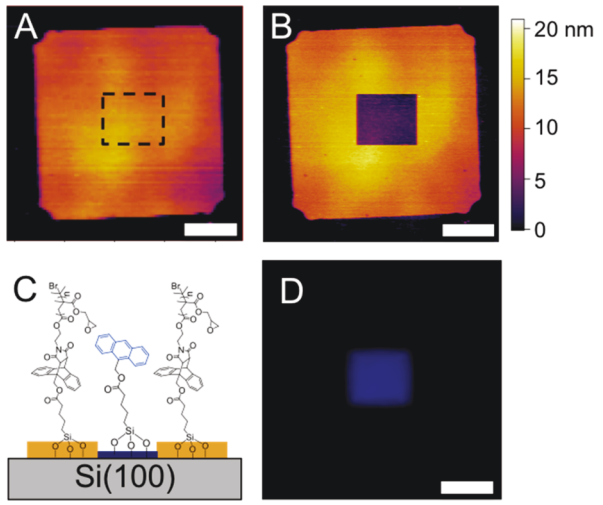

Figure 2. (A) AFM topographic image (24 × 24 μm) of a PGMA brush acquired in DMSO under 10 nN force. (B) The same area as A after the central 5.46 × 4.80 μm region was subjected to high-force (450 nN) scans at 12.52 μm/s with 256 lines. (C) The surface functionalities across the middle of image B. (D) Fluorescence microscopy image of the same region as B collected from 410 to 430 nm. All scale bars are 5.0 μm.

The successful activation of the MA mechanophores is demonstrated in Figure 2, where an 18.6 × 18.6 μm region of PGMA polymer brush is shown in the center of Figure 2A. The height of the polymer brush measures 11.4 ± 1.2 nm above the Si wafer surface. The central 5.46 × 4.80 μm region was selected to undergo a high-load (450 nN) scan in DMSO. The outcome is shown in Figure 2B, where the perturbed area appears 7.8 ± 1.3 nm lower than the surroundings or 3.5 ± 0.6 nm above the wafer surface (Figure 2C). Under excitation of a mercury lamp (centered at 360 nm), the central region exhibited fluorescence at 410−430 nm (Figure 2D), which is characteristic of anthracene (see also SI for detailed measurements).[47] The AFM and fluorescence microscopy images

DOI: 10.1021/jacs.8b10257
J. Am. Chem. Soc. 2019, 141, 4080−4085

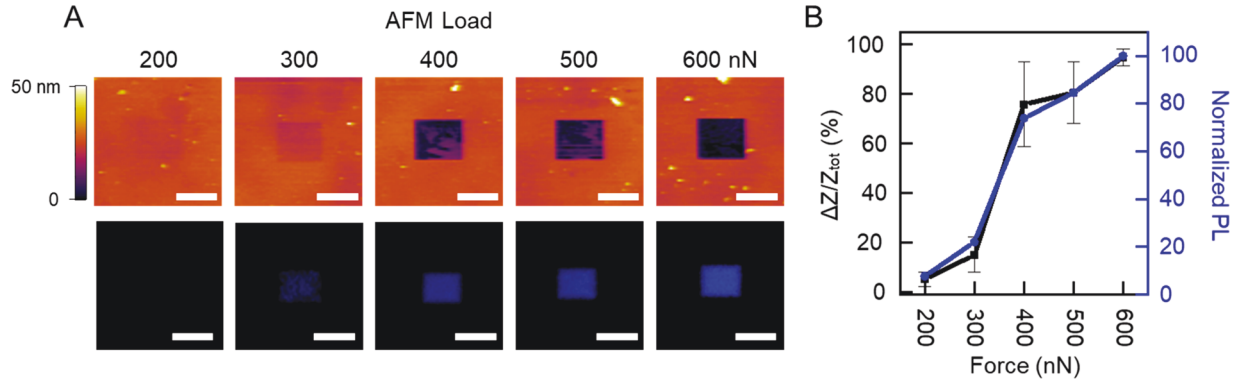

Figure 3. (A) Top: AFM topographic images of a PGMA brush on a Si wafer, taken at five designated locations. The images were acquired in DMSO under an imaging force of 55 nN. Each image covers a 15.4 × 15.4 μm area with the central 5.8 × 4.8 μm area scanned under a high load as indicated above each image. Bottom: Fluorescence microscopy images acquired at the same areas as those above. Lateral scale bars are 5.0 μm. (B) The plot shows the fluorescence intensities, normalized with respect to the 600 nN square's fluorescence (blue, Normalized PL) and relative height difference (black) as a function of load.

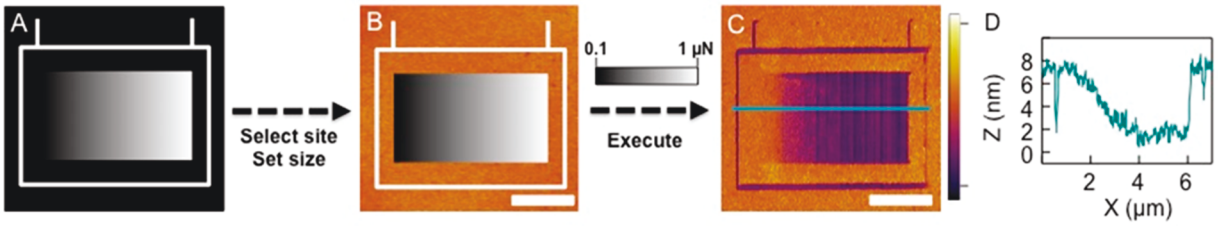

Figure 4. (A) Designed gradient image file shown in grayscale. (B) A 7.0 × 6.6 μm AFM topographic image of a PGMA brush overlaid with the physical location and dimensions of A prior to activation. AFM lithography was executed, applying the corresponding forces following the designed gradient pattern. (C) AFM topographic image of the same area as B after lithography. The polymer brush height was 10.6 ± 0.6 nm above the Si wafer surface, passivated by 1.4 ± 0.2 nm thick oligomeric ethylene oxide. The lateral scale bar and vertical range are 2.0 μm and 0−14 nm, respectively. (D) The height profile as indicated by the horizontal line in C.

verify that the interfacial MA mechanophores underwent a retro-[4 + 2] cycloaddition to generate surface-bound anthracene. Additionally, ex situ time-of-flight secondary ion mass spectroscopy (ToF-SIMS) further supports mechanophore activation (Figure S1 in SI). The high spatial selectivity is evident from Figure 2B; the feature has sharp 90°corners and straight edges.

Control experiments were performed to verify that the high local force applied triggers the retro-[4 + 2] cycloaddition of MA mechanophores without rupturing bonds elsewhere in the molecule. Identical experiments were carried out using a polymer brush, i.e., PGMA covalently linked to the Si wafer surface without a mechanophore moiety (Figure S2 in SI). The control sample was prepared following similar procedures used for fabrication of the brush in Figure 2 (see the SI for details). After being scanned under high force (450 nN), the control sample showed no discernible changes in the AFM topographic image within the force range used in this work. Fluorescence microscopy revealed no emission in the 410−430 nm region. The combined evidence from these control experiments indicates that only the weakest bonds, i.e., the MA mechanophore, were disturbed under 450 nN of force. Therefore, AFM provides a means for selective activation of interfacial MA mechanophores with high spatial fidelity.

Control over the Density of Mechanophore Activation. Given the force sensitivity of the MA mechanophores, controlling the density of mechanochemical activation is theoretically possible by varying the number and location of high-force sites within a given area. Various means are available in AFM to control the number and location of high-load sites, e.g., by controlling the line density where the probe applies a high load, employing contact at sporadic sites instead of the entire region, or reducing the local contact force, which is equivalent to reducing transient contact area.[34,53] In the example shown in Figure 3A, the outcomes under five loads (200, 300, 400, 500, or 600 nN) are compared. The PGMA polymer brush measured 26.0 ± 1.3 nm taller than the surrounding Si wafer surface. For the lowest load of 200 nN, the outline of the central region is barely discernible, and minimal fluorescence is observed, indicating that only a small portion of the MA mechanophores was activated. Between the 300 to 400 nN squares, drastic changes in both AFM topograph and the fluorescence intensity are evident. At the highest load of 600 nN, the central 5.8 × 4.8 μm region measured 24.6 ± 0.9 nm below the surrounding PGMA, and the fluorescence reached its highest intensity. Fluorescence images of the region confirmed the presence of surface-bound anthracene. Both the AFM height measurements and fluorescence intensities suggest quantitative activation of mechanophores within the scanned region, which used the deepest feature as a reference to quantify activation density as a function of AFM force (Figure 3B).

By using relative feature depth to quantify mechanophore activation density, we can further explore the mechanism of control over activation density. The height measured from AFM topography decreases with increasing MA activation, as the resulting anthracene is shorter than the PGMA brush, and thus, the remaining PGMA chains adopt a more relaxed

DOI: 10.1021/jacs.8b10257
J. Am. Chem. Soc. 2019, 141, 4080−4085

packing than the initial brush.[54,55] Assuming a linear correlation, MA mechanophore activation is estimated from height measurements and is plotted in Figure 3B,[56] and the quantification is consistent with fluorescence intensity measurements as seen from the combined plot. The control over the density of MA mechanophore activation is rationalized by the AFM probe−brush contact. A higher force manifests as a higher contact diameter, and as a larger activation area in each scan line, while the interline spacing is constant under the set scan line density. This increase in activation area per line results in an overall height decrease for the scanned area. For example, at 512 line scans covering the central 5.8 μm × 4.8 μm area, the nearest neighbor line spacing would be 9.4 nm. With a contact diameter larger than the interline spacing, complete activation of the mechanophores is expected, while reducing the load leads to contact diameters smaller than the interline spacing and, thus, a lower activation density.

Production of Complex Patterns by Design. To further test the spatial selectivity and density control, we designed and produced a gradient feature. A rectangular grayscale gradient feature was first designed and saved in bitmap format (Figure 4A). After imaging the polymer brush in DMSO at low force, a relatively flat region was selected. Then, the design from Figure 4A was input to the AFM imaging software using the program's bitmap lithography tool and applied to the selected region. The location and size of the design were adjusted to the configuration shown in Figure 4B. Then, the grayscale in the design (dark to bright) was assigned to specific loads by defining the minimum and maximum value, e.g., black = 0.1 and white = 1.0 μN, with a linear relationship for the grayscale in between. Finally, the design was transcribed onto the PGMA brush at the assigned load line-by-line. The result was imaged in contact mode in DMSO under a low force of 66 nN, as shown in Figure 4C. The gradient feature covers the central 4.8 × 2.8 μm area, requiring 351 lines and 8 min to produce. Comparing Figure 4A and C, the design was "transferred" with high fidelity in both geometry and gradient contrast. A cursor profile shown in Figure 4D indicates that the height is continuously decreasing along the x-direction during the first 2.7 μm, with the height gradient of $\Delta Z/\Delta X$ = 6.1 nm/2.7 μm = 2.26 nm/μm. Beyond 2.7 μm, the topography plateaued due to activation of all the mechanophores. The gradient can be controlled by varying the load assigned to the contrast or changing the x-range, demonstrating the feasibility and high degree of control in spatial selectivity and activation density.

The results shown in Figure 4 also facilitates the understanding of the AFM-based MA activation mechanism, e.g., pulling, normal load, or lateral shearing under high normal force. In Figure 4, for example, a series of lines were produced under increasing load. The tip remained in contact with the polymers throughout the scan. Thus, only normal force and shearing were present. The only pulling force experienced is the end contact point at the corner of the image; yet, activation was observed following the trajectory of each line, and the degree of activation is in good accordance of the normal load. In addition, we also applied normal force without lateral movement. Within the force range in this work, less than 10% activation was observed. Therefore, we infer that shearing under high load between an AFM apex and molecules under contact is primarily responsible for mechanoactivation.

A more complex design (Figure 5) was also tested. Following the same method as that in Figure 4 and defining the force range as 50−900 nN, the design was successfully replicated within the 6.15 × 6.15 μm area with two successive scans.

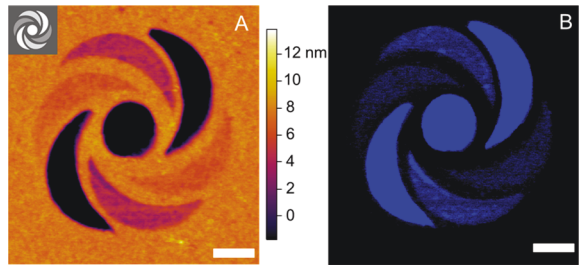

Figure 5. (A) AFM topographic image taken after scanning a complex grayscale image (inset) onto a 12.1 ± 1.3 nm thick PGMA brush immobilized by MA mechanophores on a Si wafer, passivated by 1.4 ± 0.2 nm thick oligomeric ethylene oxide. (B) Fluorescence microscopy image of the same region as A, under 360 nm excitation and collected from 410 to 430 nm. All scale bars are 1.0 μm.

The intricate geometry, such as the blades of the spiral and the central circle, were accurately produced. Even small features were replicated with high fidelity, such as the points of the blades (55 nm). Note that all the nonconnected domains, such as the blades and the central circle, were also transcribed with high fidelity without any traces of dragging. The three different shades on the blades were also faithfully "translated" by assigning the shades to different forces to be applied during the scan.

The corresponding fluorescence image was shown in Figure 5B, where the intensity map is highly consistent with the location and local abundance of anthracene termini. The robustness of high spatial selectivity was verified by production of a hierarchical feature (e.g., the rectangular feature in the TOC). Results from Figures 4 and 5 demonstrate that combining AFM with the mechanochemical reaction led to high fidelity and spatial accuracy. Such a high degree of control and selectivity paves the way for a broad range of applications, including composite material engineering, molecular control over the chemical and physical properties of surfaces, and fabrication of stress-sensitive nano devices.[1,2,43,44]

■ CONCLUSIONS

We demonstrate the activation of a surface immobilized maleimide−anthracene mechanophore with a PGMA brush using AFM. Taking advantage of the accurate force control in AFM, the contact force between the probe apex and the substrate-bound mechanophore was tuned for either imaging or activation. The retro-[4 + 2] cycloaddition upon activation of the MA mechanophore was verified by the topographic changes revealed by in situ AFM imaging and fluorescence microscopy, where surface-bound anthracene exhibits a characteristic emission at 410−430 nm. This new means to activate mechanophores has the intrinsic advantages of (a) a wide range of force control and tunability; (b) high spatial precision, which enables nanolithography (we focused on utilizing AFM nanolithography); and (c) in situ activation and characterization. The high spatial resolution of AFM enabled nanolithography of complex structures with high spatial accuracy and selectivity. Unlike prior 2D nanolithography where the contrast is mostly binary, we demonstrate that multilevel contrast in the original design, including gradient features and hierarchical micro and nanostructures, could be

DOI: 10.1021/jacs.8b10257
J. Am. Chem. Soc. 2019, 141, 4080−4085

faithfully translated via spatially controlled surface chemistry. The concept and methodology developed in this work is of generic importance for other mechanophore containing materials. Work is in progress to construct 3D nanostructures by combing this approach with subsequent surface reactions, which will enable 3D nanoprinting. Future applications include production of coatings and composite materials that require nanopatterning or texture control as well as nanodevices and sensors for measuring mechanical stress and damages in situ.

■ ASSOCIATED CONTENT

Supporting Information

The Supporting Information is available free of charge on the ACS Publications website at DOI: 10.1021/jacs.8b10257.

Experimental details, synthetic procedures, ToF-SIMS data, optical microscopy data, additional fluorescence data, and testing of control samples (PDF)

■ AUTHOR INFORMATION

Corresponding Authors

*gyliu@ucdavis.edu (G.-y.L.)
*n-sottos@illinois.edu (N.R.S.)

ORCID

Audrey R. Sulkanen: 0000-0002-7863-2484
Maxwell J. Robb: 0000-0002-0528-9857
Nancy R. Sottos: 0000-0002-5818-520X
Gang-yu Liu: 0000-0003-3689-0685

Author Contributions

#A.R.S. and J.S. contributed equally to this work.

Notes

The authors declare no competing financial interest.

■ ACKNOWLEDGMENTS

We thank Dr. Jun Li at UIUC and Ms. Yunbo Zheng at UC Davis for helpful scientific discussions and Dr. Logan Swartz at UC Davis for technical assistance. This work was supported by the Gordon and Betty Moore Foundation, the National Science Foundation (DMR 13-07354 and CHE-1808829), and the Office of Naval Research (Grant No. 0014-12-1-0828). M.J.R. gratefully acknowledges the Arnold and Mabel Beckman Foundation for a Beckman Institute Postdoctoral Fellowship.

■ REFERENCES

(1) Li, J.; Nagamani, C.; Moore, J. S. Polymer Mechanochemistry: From Destructive to Productive. *Acc. Chem. Res.* **2015**, *48*, 2181−2190.

(2) Black, A. L.; Lenhardt, J. M.; Craig, S. L. From molecular mechanochemistry to stress-responsive materials. *J. Mater. Chem.* **2011**, *21*, 1655−1663.

(3) Brantley, J. N.; Wiggins, K. M.; Bielawski, C. W. Polymer mechanochemistry: the design and study of mechanophores. *Polym. Int.* **2013**, *62*, 2−12.

(4) Allison, D. P.; Hinterdorfer, P.; Han, W. H. Biomolecular force measurements and the atomic force microscope. *Curr. Opin. Biotechnol.* **2002**, *13*, 47−51.

(5) Robb, M. J.; Kim, T. A.; Halmes, A. J.; White, S. R.; Sottos, N. R.; Moore, J. S. Regioisomer-Specific Mechanochromism of Naphthopyran in Polymeric Materials. *J. Am. Chem. Soc.* **2016**, *138*, 12328−12331.

(6) Davis, D. A.; Hamilton, A.; Yang, J.; Cremar, L. D.; Van Gough, D.; Potisek, S. L.; Ong, M. T.; Braun, P. V.; Martinez, T. J.; White, S. R.; Moore, J. S.; Sottos, N. R. Force-induced activation of covalent bonds in mechanoresponsive polymeric materials. *Nature* **2009**, *459*, 68−72.

(7) Gossweiler, G. R.; Hewage, G. B.; Soriano, G.; Wang, Q.; Welshofer, G. W.; Zhao, X.; Craig, S. L. Mechanochemical activation of covalent bonds in polymers with full and repeatable macroscopic shape recovery. *ACS Macro Lett.* **2014**, *3*, 216−219.

(8) Piermattei, A.; Karthikeyan, S.; Sijbesma, R. P. Activating catalysts with mechanical force. *Nat. Chem.* **2009**, *1*, 133−137.

(9) Diesendruck, C. E.; Peterson, G. I.; Kulik, H. J.; Kaitz, J. A.; Mar, B. D.; May, P. A.; White, S. R.; Martínez, T. J.; Boydston, A. J.; Moore, J. S. Mechanically triggered heterolytic unzipping of a low-ceiling-temperature polymer. *Nat. Chem.* **2014**, *6*, 623−628.

(10) Larsen, M. B.; Boydston, A. J. "Flex-activated" mechanophores: using polymer mechanochemistry to direct bond bending activation. *J. Am. Chem. Soc.* **2013**, *135*, 8189−8192.

(11) Chen, Z.; Mercer, J. A.; Zhu, X.; Romaniuk, J. A.; Pfattner, R.; Cegelski, L.; Martinez, T. J.; Burns, N. Z.; Xia, Y. Mechanochemical unzipping of insulating polyladderene to semiconducting polyacetylene. *Science* **2017**, *357*, 475−479.

(12) Li, J.; Shiraki, T.; Hu, B.; Wright, R. A.; Zhao, B.; Moore, J. S. Mechanophore activation at heterointerfaces. *J. Am. Chem. Soc.* **2014**, *136*, 15925−15928.

(13) Imato, K.; Natterodt, J. C.; Sapkota, J.; Goseki, R.; Weder, C.; Takahara, A.; Otsuka, H. Dynamic covalent diarylbibenzofuranone-modified nanocellulose: mechanochromic behaviour and application in self-healing polymer composites. *Polym. Chem.* **2017**, *8*, 2115−2122.

(14) Woodcock, J. W.; Beams, R.; Davis, C. S.; Chen, N.; Stranick, S. J.; Shah, D. U.; Vollrath, F.; Gilman, J. W. Observation of Interfacial Damage in a Silk-Epoxy Composite, Using a Simple Mechanoresponsive Fluorescent Probe. *Adv. Mater. Interfaces* **2017**, *4*, 1601018.

(15) Beiermann, B. A.; Kramer, S. L. B.; May, P. A.; Moore, J. S.; White, S. R.; Sottos, N. R. The Effect of Polymer Chain Alignment and Relaxation on Force-Induced Chemical Reactions in an Elastomer. *Adv. Funct. Mater.* **2014**, *24*, 1529−1537.

(16) Kim, T. A.; Beiermann, B. A.; White, S. R.; Sottos, N. R. Effect of Mechanical Stress on Spiropyran-Merocyanine Reaction Kinetics in a Thermoplastic Polymer. *ACS Macro Lett.* **2016**, *5*, 1312−1316.

(17) Potisek, S. L.; Davis, D. A.; Sottos, N. R.; White, S. R.; Moore, J. S. Mechanophore-linked addition polymers. *J. Am. Chem. Soc.* **2007**, *129*, 13808−13809.

(18) May, P. A.; Munaretto, N. F.; Hamoy, M. B.; Robb, M. J.; Moore, J. S. Is Molecular Weight or Degree of Polymerization a Better Descriptor of Ultrasound-Induced Mechanochemical Transduction? *ACS Macro Lett.* **2016**, *5*, 177−180.

(19) Berkowski, K. L.; Potisek, S. L.; Hickenboth, C. R.; Moore, J. S. Ultrasound-induced site-specific cleavage of azo-functionalized poly (ethylene glycol). *Macromolecules* **2005**, *38*, 8975−8978.

(20) Gossweiler, G. R.; Kouznetsova, T. B.; Craig, S. L. Force-rate characterization of two spiropyran-based molecular force probes. *J. Am. Chem. Soc.* **2015**, *137*, 6148−6151.

(21) Kersey, F. R.; Yount, W. C.; Craig, S. L. Single-molecule force spectroscopy of bimolecular reactions: system homology in the mechanical activation of ligand substitution reactions. *J. Am. Chem. Soc.* **2006**, *128*, 3886−3887.

(22) Wang, J. P.; Kouznetsova, T. B.; Niu, Z. B.; Ong, M. T.; Klukovich, H.; Rheingold, A. L.; Martinez, T. J.; Craig, S. L. Inducing and quantifying forbidden reactivity with single-molecule polymer mechanochemistry. *Nat. Chem.* **2015**, *7*, 323−327.

(23) Zou, S.; Schonherr, H.; Vancso, G. J. Stretching and rupturing individual supramolecular polymer chains by AFM. *Angew. Chem., Int. Ed.* **2005**, *44*, 956−959.

(24) Klukovich, H. M.; Kouznetsova, T. B.; Kean, Z. S.; Lenhardt, J. M.; Craig, S. L. A backbone lever-arm effect enhances polymer mechanochemistry. *Nat. Chem.* **2013**, *5*, 110−114.

(25) Sung, J.; Robb, M. J.; White, S. R.; Moore, J. S.; Sottos, N. R. Interfacial Mechanophore Activation Using Laser-Induced Stress Waves. *J. Am. Chem. Soc.* **2018**, *140*, 5000−5003.

DOI: 10.1021/jacs.8b10257
J. Am. Chem. Soc. 2019, 141, 4080−4085

(26) Liu, M.; Amro, N. A.; Liu, G.-y. Nanografting for surface physical chemistry. *Annu. Rev. Phys. Chem.* **2008**, *59*, 367−386.
(27) Kaholek, M.; Lee, W. K.; LaMattina, B.; Caster, K. C.; Zauscher, S. Fabrication of stimulus-responsive nanopatterned polymer brushes by scanning-probe lithography. *Nano Lett.* **2004**, *4*, 373−376.
(28) Carpick, R. W.; Salmeron, M. Scratching the surface: Fundamental investigations of tribology with atomic force microscopy. *Chem. Rev.* **1997**, *97*, 1163−1194.
(29) Drake, B.; Prater, C. B.; Weisenhorn, A. L.; Gould, S. A. C.; Albrecht, T. R.; Quate, C. F.; Cannell, D. S.; Hansma, H. G.; Hansma, P. K. Imaging Crystals, Polymers, and Processes in Water with the Atomic Force Microscope. *Science* **1989**, *243*, 1586−1589.
(30) Vezenov, D. V.; Noy, A.; Ashby, P. Chemical force microscopy: probing chemical origin of interfacial forces and adhesion. *J. Adhes. Sci. Technol.* **2005**, *19*, 313−364.
(31) Garcia-Manyes, S.; Sanz, F. Nanomechanics of lipid bilayers by force spectroscopy with AFM: A perspective. *Biochim. Biophys. Acta, Biomembr.* **2010**, *1798*, 741−749.
(32) Fisher, T. E.; Oberhauser, A. F.; Carrion-Vazquez, M.; Marszalek, P. E.; Fernandez, J. M. The study of protein mechanics with the atomic force microscope. *Trends Biochem. Sci.* **1999**, *24*, 379−384.
(33) Ludwig, M.; Rief, M.; Schmidt, L.; Li, H.; Oesterhelt, F.; Gautel, M.; Gaub, H. E. AFM, a tool for single-molecule experiments. *Appl. Phys. A: Mater. Sci. Process.* **1999**, *68*, 173−176.
(34) Syed Asif, S. A. S.; Wahl, K. J.; Colton, R. J.; Warren, O. L. Quantitative imaging of nanoscale mechanical properties using hybrid nanoindentation and force modulation. *J. Appl. Phys.* **2001**, *90*, 1192.
(35) Liu, J. F.; Cruchon-Dupeyrat, S.; Garno, J. C.; Frommer, J.; Liu, G. Y. Three-dimensional nanostructure construction via nanografting: Positive and negative pattern transfer. *Nano Lett.* **2002**, *2*, 937−940.
(36) Xu, S.; Laibinis, P. E.; Liu, G. Y. Accelerating the kinetics of thiol self-assembly on gold - A spatial confinement effect. *J. Am. Chem. Soc.* **1998**, *120*, 9356−9361.
(37) Liu, M.; Amro, N. A.; Liu, G. Y. Nanografting for surface physical chemistry. *Annu. Rev. Phys. Chem.* **2008**, *59*, 367−386.
(38) Liu, G. Y.; Amro, N. A. Positioning protein molecules on surfaces: A nanoengineering approach to supramolecular chemistry. *Proc. Natl. Acad. Sci. U. S. A.* **2002**, *99*, 5165−5170.
(39) Xu, S.; Liu, G. Y. Nanometer-scale fabrication by simultaneous nanoshaving and molecular self-assembly. *Langmuir* **1997**, *13*, 127−129.
(40) Piner, R. D.; Zhu, J.; Xu, F.; Hong, S. H.; Mirkin, C. A. "Dip-pen" nanolithography. *Science* **1999**, *283*, 661−663.
(41) Maoz, R.; Frydman, E.; Cohen, S. R.; Sagiv, J. "Constructive nanolithography": Inert monolayers as patternable templates for in-situ nanofabrication of metal-semiconductor-organic surface structures - A generic approach. *Adv. Mater.* **2000**, *12*, 725.
(42) Zhou, X. C.; Liu, Z. L.; Xie, Z.; Liu, X. Q.; Zheng, Z. J. High-Resolution, Large-Area, Serial Fabrication of 3D Polymer Brush Structures by Parallel Dip-Pen Nanodisplacement Lithography. *Small* **2012**, *8*, 3568−3572.
(43) Frazier, W. E. Metal Additive Manufacturing: A Review. *J. Mater. Eng. Perform.* **2014**, *23*, 1917−1928.
(44) Ivanova, O.; Williams, C.; Campbell, T. Additive manufacturing (AM) and nanotechnology: promises and challenges. *Rapid Prototyping J.* **2013**, *19*, 353−364.
(45) Nofen, E. M.; Dasgupta, A.; Zimmer, N.; Gunckel, R.; Koo, B.; Chattopadhyay, A.; Dai, L. L. Universal Stress-Sensing Dimeric Anthracene-Based Mechanophore Particle Fillers Incorporated into Polyurethane Thermoset Matrices. *Polym. Eng. Sci.* **2017**, *57*, 901−909.
(46) Li, J.; Hu, B.; Yang, K.; Zhao, B.; Moore, J. S. Effect of Polymer Grafting Density on Mechanophore Activation at Heterointerfaces. *ACS Macro Lett.* **2016**, *5*, 819−822.
(47) Li, H.; Göstl, R.; Delgove, M.; Sweeck, J.; Zhang, Q.; Sijbesma, R. P.; Heuts, J. P. A. Promoting Mechanochemistry of Covalent Bonds by Noncovalent Micellar Aggregation. *ACS Macro Lett.* **2016**, *5*, 995−998.
(48) Church, D. C.; Peterson, G. I.; Boydston, A. J. Comparison of Mechanochemical Chain Scission Rates for Linear versus Three-Arm Star Polymers in Strong Acoustic Fields. *ACS Macro Lett.* **2014**, *3*, 648−651.
(49) Ulman, A. Formation and structure of self-assembled monolayers. *Chem. Rev.* **1996**, *96*, 1533−1554.
(50) Liu, G. Y.; Xu, S.; Qian, Y. L. Nanofabrication of self-assembled monolayers using scanning probe lithography. *Acc. Chem. Res.* **2000**, *33*, 457−466.
(51) Drexler, C. I.; Moore, K. B.; Causey, C. P.; Mullen, T. J. Atomic Force Microscopy Characterization and Lithography of Cu-Ligated Mercaptoalkanoic Acid "Molecular Ruler" Multilayers. *Langmuir* **2014**, *30*, 7447−7455.
(52) Hirtz, M.; Brinks, M. K.; Miele, S.; Studer, A.; Fuchs, H.; Chi, L. F. Structured Polymer Brushes by AFM Lithography. *Small* **2009**, *5*, 919−923.
(53) Helt, J. M.; Batteas, J. D. Implications of the contact radius to line step (CRLS) ratio in AFM for nanotribology measurements. *Langmuir* **2006**, *22*, 6130−6141.
(54) Milner, S. Polymer brushes. *Science* **1991**, *251*, 905−914.
(55) Chen, T.; Amin, I.; Jordan, R. Patterned polymer brushes. *Chem. Soc. Rev.* **2012**, *41*, 3280−3296.
(56) Zhou, T.; Qi, H.; Han, L.; Barbash, D.; Li, C. Y. Towards controlled polymer brushes via a self-assembly-assisted-grafting-to approach. *Nat. Commun.* **2016**, *7*, 11119.

DOI: 10.1021/jacs.8b10257
J. Am. Chem. Soc. 2019, 141, 4080−4085